Integrated photoacoustic, confocal, and two-photon microscope

Bin Rao
Florentina Soto
Daniel Kerschensteiner
Lihong V. Wang

Integrated photoacoustic, confocal, and two-photon microscope

Bin Rao,[a] Florentina Soto,[b] Daniel Kerschensteiner,[b] and Lihong V. Wang[a,*]
[a]Washington University in St. Louis, Optical Imaging Laboratory, Department of Biomedical Engineering, One Brookings Drive, St. Louis, Missouri 63130
[b]Washington University School of Medicine, Department of Ophthalmology and Visual Sciences, Box 8096, St. Louis, Missouri 63110

Abstract. The invention of green fluorescent protein and other molecular fluorescent probes has promoted applications of confocal and two-photon fluorescence microscopy in biology and medicine. However, exogenous fluorescence contrast agents may affect cellular structure and function, and fluorescence microscopy cannot image nonfluorescent chromophores. We overcome this limitation by integrating optical-resolution photoacoustic microscopy into a modern Olympus IX81 confocal, two-photon, fluorescence microscope setup to provide complementary, label-free, optical absorption contrast. Automatically coregistered images can be generated from the same sample. Imaging applications in ophthalmology, developmental biology, and plant science are demonstrated. For the first time, in a familiar microscopic fluorescence imaging setting, this trimodality microscope provides a platform for future biological and medical discoveries. © *2014 Society of Photo-Optical Instrumentation Engineers (SPIE)* [DOI: 10.1117/1.JBO.19.3.036002]

1 Introduction

Fluorescent proteins (FP) are structural homologs of *Aequorea* green fluorescent protein (GFP), and they are able to form an internal visible wavelength fluorophore from their own polypeptide sequence. Since Chalfie et al. first successfully demonstrated the significant potential of GFP as a molecular fluorescent probe,[1] confocal fluorescence microscopy has been widely used to monitor gene expression and protein localization in living organisms. The development of genetic mutation technologies resulted in enhanced GFP and variously colored mutants, such as blue (BFP), cyan (CFP), yellow (YFP), and their enhanced versions (EBFP, ECFP, and EYFP).[2] The enriched contrast mechanisms provided by these fluorescent proteins further promoted the usage of confocal fluorescence microscopy. The evolution from confocal technology to two-photon microscopy provided higher contrast, lower toxicity, and deeper imaging depth due to the unique two-photon excitation approach. Even more recently developed optical-resolution photoacoustic microscopy (OR-PAM) extends microscopy technology further to image nonfluorescent chromophores, such as hemoglobin, melanin, cytochromes, and lipids.[3–5] Functional OR-PAM reveals the physiological status of an organism by probing the optical absorption of nonfluorescent proteins at different wavelengths.[2] There should be other, unknown, nonfluorescent light absorbing chromophores that can serve as reporters for various vital biological processes. Our previously reported integrated confocal and OR-PAM imaging system[6–8] and other similar systems[4,9–11] are not suitable for biologic discovery because (1) they do not have flexibility in the selection of objectives, fluorescence dyes, filter sets, and some of the complementary imaging modes, such as bright-field imaging, wide-field epi-fluorescence imaging, and differential interference contrast (DIC) imaging, which are

provided in a modern fluorescence microscope, and (2) they do not provide two-photon microscopy, the most important fluorescence microscopy technology. No modern microscope that can image both fluorescent proteins and nonfluorescent chromophores with confocal, two-photon, and PA technologies exists for biologists and physicians. Here, we report the development of an automatically coregistered trimodality microscope that fills this gap. In a familiar microscopic fluorescence imaging setting, this microscope provides the research community with a novel platform for future biological and medical discoveries.

2 Material and Methods

2.1 Microscope System

We built this microscope on a commercial Olympus inverted setup (IX81). It integrates confocal, two-photon, and OR-PAM imaging in a single platform, as shown in Fig. 1(a). A femtosecond laser (Mai Tai®, Spectra-Physics, Santa Clara, California) is used for two-photon excitation. Several continuous-wave (CW) laser beams of 405, 488, 543, and 635 nm wavelengths are provided by a CW laser unit (not shown in Fig. 1) and coupled to a microscope visible port via a single-mode optical fiber (not shown in Fig. 1). An acousto-optic tunable filter in the CW laser unit can simultaneously output any combination of these laser lines with different attenuations. The collimated laser beams for confocal imaging share the same visible port with a tunable dye laser (Credo, Sirah Lasertechik GmbH, Grevenbroich, Germany) operating at a pulse repetition rate of 10 kHz for PA imaging. Currently, with a pump laser of 532 nm, a 541- to 900-nm wavelength range is covered with different dye settings. Alternatively, a dye laser range between 372 and 722 nm could be acquired if a pump laser wavelength of

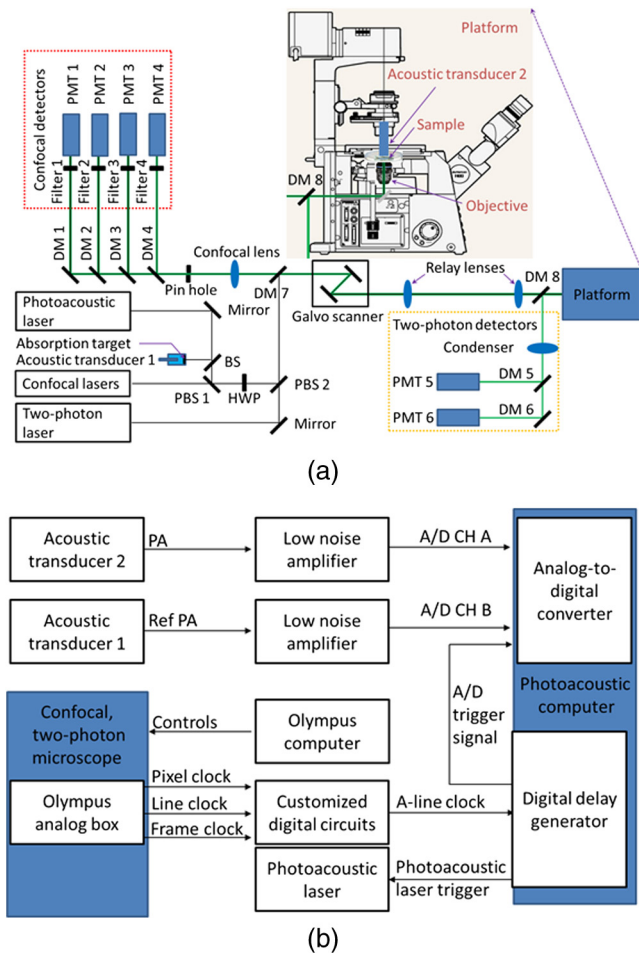*Address all correspondence to: Lihong V. Wang, E-mail: lhwang@wustl.edu

Fig. 1 (a) Schematic of the integrated confocal, two-photon, and optical-resolution photoacoustic microscope. BS, beam splitter; DM, dichroic mirror; DMW, dichroic mirror wheel; HWP, half-wave plate; PBS, polarization beam splitter; PMT, photomultiplier tube. (b) Logic function of the integrated confocal, two-photon, and optical-resolution photoacoustic microscope system.

platform (IX81, Olympus America Inc, Center Valley, Pennsylvania). The inset in Fig. 1(a) is a schematic of the IX81 platform. The forward-propagating PA wave excited by the dye laser beam is detected by acoustic transducer 2 whose focus overlaps the region of interest in the sample. The backward-propagating fluorescent light excited by either the confocal or two-photon laser beam is detected by one of the two groups of photomultiplier tube (PMT) detectors. One group of optical filters and photomultipliers detects fluorescence excited by the confocal lasers, and the other group detects fluorescence excited by the two-photon laser. A pin-hole at the focus of a confocal lens is optically conjugated with the focus of the objective in the sample. The pin-hole improves fluorescence image contrast by rejecting background fluorescence signals. The pin-hole is not necessary for two-photon fluorescence detection, which excites fluorescence signals only from the tight focus of the objective. Dichroic mirrors (DM 7 and DM 8) can be selected in the microscope's software. For two-photon microscopy, dichroic mirror RDM690 is selected at the DM 8 location, and a second dichroic mirror is selected at the DM 7 location. For confocal fluorescence microscopy, no dichroic mirror is selected at the DM 8 location, and different dichroic mirrors are selected at the DM 7 location according to the fluorescence dye settings. When a 20:80 (reflection:transmission) beam splitter is chosen at the DM 7 location and no filters are selected in front of the confocal PMT detectors, the confocal fluorescence microscope senses optical scattering instead of fluorescence. For PAM, no dichroic mirror is selected at the DM 8 location, and a highly reflective mirror is selected at the DM 7 location. Similarly, different dichroic mirrors will be selected in the software settings for DM 1 to 4 fluorescence detection locations. For two-photon microscopy, three different dichroic mirror sets can be selected and manually installed at the DM 5 and DM 6 locations.

In conventional modes, this microscope also supports bright-field imaging, wide-field epi-fluorescence imaging, and DIC imaging, which are not shown in the schematic. A beam profiling device is used to align the OR-PAM imaging focus with the confocal laser beam focus and two-photon laser focus. The aligned trifoci guarantee the coregistration of three modality images.

The OR-PAM imaging mode is implemented passively as shown in Fig. 1(b): an independent PA computer (Dell workstation T1600) listens to the synchronization signals sent from the analog box of the Olympus microscope system and acquires PA signals from the acoustic transducers. Pixel, line, and frame clocks are digital pulses that signal the beginning of a pixel, a line, and a frame in the scanning protocol. These digital pulses are connected to a customized digital circuit that synthesizes an A-line trigger signal for PAM imaging mode. This A-line trigger signal is passed to a delay generator to generate an external dye laser trigger signal and a data acquisition card trigger signal. The PA signals from the acoustic transducers are simultaneously digitized with an analog-to-digital converter during PAM imaging.

A hybrid scanning protocol, including both optical scanning within the acoustic focal zone and mechanical scanning in both x and y directions, is adopted for the OR-PAM imaging mode; it is implemented by the Olympus's Multiple Area Time Lapse add-on software. In the following OR-PAM imaging demonstrations, a large imaging field of view is divided into an N by N matrix. Within each matrix element, an optical scan is performed. PA signals from the two acoustic transducers are amplified with low-noise amplifiers (Mini-circuit ZFL-500) and

355 nm was used. This wide laser wavelength tuning capability is the key to exploring both endogenous and exogenous optical absorption contrast mechanisms in biological applications.

In this new microscope, a polarization beam splitter (PBS 1) allows the insertion of a dye laser beam for PAM into the optical path of the confocal laser beams. A two-photon laser beam is combined with the confocal laser beams via another polarization beam splitter (PBS 2). A half-wave plate (HWP) inserted after PBS 1 maximizes the light intensity passing through PBS 2 by adjusting its orientation to two different angles for the confocal laser and dye laser beams. To switch between confocal and PA imaging, the orientation angle of the HWP is adjusted. To compensate for fluctuations of the pulsed dye laser output, a beam splitter (BS) directs a fraction of the dye laser's energy to a known absorption target in front of acoustic transducer 1, which monitors the laser pulse energy by detecting the PA signal generated from the absorption target. This PA signal, as a reference PA signal, also calibrates the absorption coefficient of the sample.

The confocal, two-photon, or PA excitation laser beam is reflected by a dichroic mirror (DM 7) and a pair of galvo mirrors. The center point between the two galvo mirrors is imaged by a pair of relay lens to the pupil of the objective in the imaging

acquired via two analog input channels of an analog-to-digital card (AlazarTech ATS-9350). A customized LabVIEW program running on the independent Dell workstation acquires, saves, and processes OR-PAM data, while the Olympus software running on the Olympus computer initiates and controls the hybrid scanning protocol. A 100-μs integration time for each pixel in the Olympus software configuration is chosen for the OR-PAM imaging mode.

2.2 Sample Preparations and Microscope Settings

In the first demonstration, we imaged a sectioned transgenic mouse retina. The mouse eyecup preparation followed the protocol described in a previous publication.[12] The eyecup was then cryoprotected, frozen, and vertically cut into 2-μm-thick slices. Retinal tissue slices were placed on top of a 1-mm-thick microscope slide, covered with a thin plastic cover slip, and sealed with colorless nail polish. We drilled an opening in the bottom of a plastic petri dish. Then, we used vacuum grease to attach the slide to the bottom of the dish and seal the gap between the slide and dish. Then we filled the dish with deionized (DI) water and immersed the receiving end of the acoustic transducer. The transgenic mouse used in this study expressed an attenuated version of diphtheria toxin (DTA) driven by a receptor promoter specific to depolarizing-to-light-onset (ON) bipolar cells (mGluR6 promoter) in a Cre-dependent manner (*Grm6::loxP-YFPstop-loxP-DTA*, *DTA* mice). In the absence of Cre-mediated recombination, YFP (but not DTA) was expressed by ON bipolar cells.

In the confocal imaging software settings, we selected Olympus UPlanFLN 40× (NA 0.6), Alexa Fluor 488, dichroic mirror DM 405/488, and band-pass filter BA 505-605. A confocal fluorescence image was acquired at 488 nm excitation wavelength. A 317.1 μm by 317.1 μm image field of view was scanned to form an image of 1280 by 1280 pixels. To observe the convention in neural science, the confocal image was rotated in ImageJ software to make the ganglion cell layer at the bottom. An OR-PAM maximum amplitude projection (MAP) image was acquired subsequently with the same objective, using a dye laser wavelength of 570 nm and laser pulse energy of 100 nJ per pulse. The same imaging field of view was divided into a 10 by 10 matrix with an element size of 31.71 μm by 31.71 μm. The data acquisition time for the entire matrix (1280 by 1280 pixels) was 18 min. Again, the OR-PAM image was rotated.

Next, we imaged a zebrafish embryo[13] *in vivo* as a demonstration of a developmental biology application. A 7-dpf zebrafish embryo was acquired from Washington University's zebrafish facility and prepared in a petri dish with a previously published agar mounting method.[14] Additional embryo medium was added to immerse the acoustic transducer. For confocal imaging, we selected the Olympus UPlanFLN 10× (NA 0.3) objective, Alexa Fluor 488, dichroic mirror DM 405/488, and band-pass filter BA 505-605. An image field of view of 317.6 μm by 317.6 μm was scanned to form an image of 640 by 640 pixels near the zebrafish's trunk area. A series of seven confocal images was acquired from different depths with 50 μm axial separation. To render a projected confocal image, Z projection using the maximum intensity algorithm in ImageJ software was performed. Next, from different depths with 50 μm axial separation, we acquired a series of eight OR-PAM MAP images with the same objective, using a dye laser wavelength of 570 nm and laser pulse energy of 100 nJ per pulse. The same imaging field of view was divided into a 10 by 10 matrix with an element size of 31.76 μm by 31.76 μm. Once again, to render

a projected PA image, we performed Z projection using the maximum intensity algorithm in ImageJ software. The data acquisition time for the entire matrix (640 by 640 pixels) at one imaging depth was 11 min and 10 s. The total data acquisition time for the OR-PAM imaging data at eight depths was 89 min and 20 s, excluding the manual software operation time.

The last sample we imaged was wild-type moss leaves acquired from a rock near a freshwater pond. Rhizoids were cut from the leaves by a surgical blade. Then the leaves were laid inside a petri dish with a glass cover glass at its bottom. A drop of pond water was applied on top of the sample. Clear adhesive tape flattened and fixed the leaves on the cover glass. Then, the dish was filled with DI water to immerse the acoustic transducer. Four lasers (a Mai-Tai® femtosecond laser at 800 nm, a confocal laser at 635 nm, a nanosecond dye laser at 570 nm, and a nanosecond dye laser at 578 nm) were used sequentially for two-photon, confocal, and OR-PAM microscopy. The Olympus UPlanFLN 40× objective (NA 0.6) was used for all imaging modalities. An imaging field of view of 317.1 μm by 317.1 μm was scanned to form an image of 1024 by 1024 pixels. For the Olympus software settings for two-photon imaging, we selected 800 nm excitation, dichroic mirror RDM690, and no filter in front of the two-photon PMT detectors. The Olympus software setting for confocal imaging included excitation at 635 nm, dichroic mirror DM405/488/543/635, Alexa Fluor 633 dye, and band-pass filter BA 655-755. For OR-PAM imaging, we selected a matrix of 8 by 8 with element size of 39.64 μm by 39.64 μm and a customized highly reflective mirror as the dichroic mirror. The data acquisition time for the entire matrix (1024 by 1024 pixels) was 11 min and 31.3 s.

3 Results and Discussions

The imaging results of the sectioned transgenic mouse retina are shown in Fig. 2. In the confocal image [Fig. 2(a)], the small bright dots in the inner and outer segments (IOS) layer are the light sensing segments of photoreceptor cells (rods or cones). The cell bodies of rods or cones are located in the outer nuclear layer. The connections between photoreceptor cells and bipolar cells are located in the outer plexiform layer. The bright cell bodies shown in the inner nuclear layer (INL) are labeled bipolar cells. Horizontal cells and amacrine cells in the INL are not visible. Bipolar cells form connections with ganglion cells in the inner plexiform layer. Ganglion cells in the ganglion cell layer were not labeled in this mouse. The separation between IOS and retinal pigmented layers is caused by the processing of tissue. The light sensing neuron signal was initiated by photoreceptor cells, then processed by horizontal cells, bipolar cells, and amacrine cells, and finally carried by ganglion cells through their axons that form the optic nerve connected to the brain. Some neural circuits may not function properly due to the degeneration of photoreceptor cells in an eye with age-related macular degeneration (AMD). The retinal pigmented epithelium (RPE) layer shown in the OR-PAM MAP image [Fig. 2(b)] nourishes the retina and phagocytoses the oldest outer segment discs of the photoreceptors. It is widely accepted that the pigmentary changes observed in AMD cases are attributable to degenerative changes in the highly melanized RPE cells, which are accompanied by concomitant photoreceptor degenerations. Imaging both retinal neuronal cells and RPE cells using dual-modality confocal microscopy and PAM [Fig. 2(c)] might be useful in studying AMD diseases
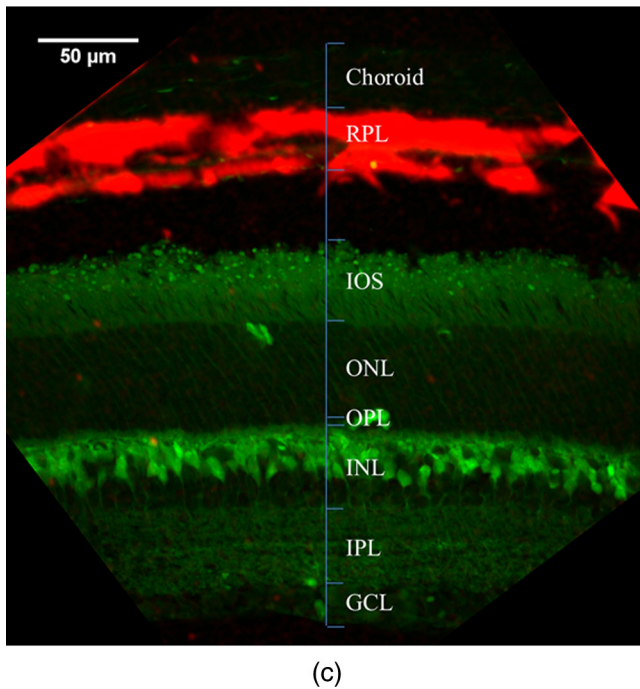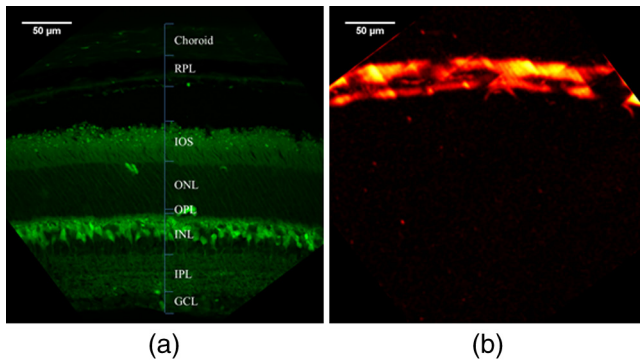
(a)

(b)

(c)

Fig. 2 A transgenic mouse retinal slice imaged by confocal and optical-resolution photoacoustic microscopy. In the confocal retinal image (a), retinal layers, retinal pigmented layer, and chroid are labeled. The small bright dots in the inner and outer segments layer are the light sensing segments of photoreceptor cells (rods or cones). In the inner nuclear layer, the bright cell bodies of the ON bipolar cells can be seen. Melanin in retinal pigmented layers gives strong signals in the optical-resolution photoacoustic microscopy (OR-PAM) image (b). In the merged image (c), the confocal fluorescent image is shown in green and the photoacoustic absorption contrast image is shown in red. GCL, ganglion cell layer; INL, inner nuclear layer; IOS, inner and outer photoreceptor segments; IPL, inner plexiform layer; ONL, outer nuclear layer; OPL, outer plexiform layer.

(a)

(b)

(c)

Fig. 3 Maximum intensity Z-projection images from a series of confocal and OR-PAM images acquired *in vivo* from a zebrafish embryo at different depths. The ventral tract of spinal cord, posterior lateral line nerve, and bright interneuron-like cells are shown in the maximum intensity Z projection image (a) of these confocal images. The dorsal longitudinal anastomotic vessel (DLAV), caudal artery (CA), caudal vein (CV), and inter-segmental vessel (Se) are shown in the maximum intensity Z projection image (b) of these photoacoustic images of the vasculature system at the trunk of the zebrafish. Melanin (Mn) in the skin forms a pattern in the background of (b). The merged image (c) shows both neural and vasculature components with fluorescence and optical absorption contrast.

in animal models and in developing novel treatment or drugs for AMD diseases.

The *in vivo* imaging results of the zebrafish are shown in Fig. 3. The ventral tract of the spinal cord, the posterior lateral line nerve, and bright interneuron-like cells are shown in the maximum intensity Z projection image [Fig. 3(a)]. Components of the blood vessel system in the trunk of the zebrafish, which are identified in Fig. 3(b), include the dorsal longitudinal anastomotic vessel, caudal artery, caudal vein, and intersegmental vessel. Melanin in the skin forms a pattern in the background of Fig. 3(b). Both neuron components and vasculature components of the trunk of an *in vivo* zebrafish can be visualized in the merged dual-contrast image shown in Fig. 3(c).
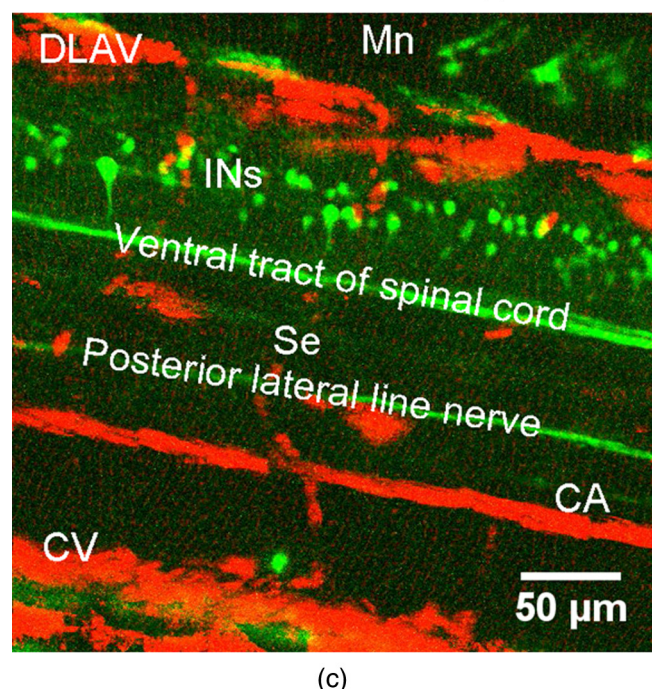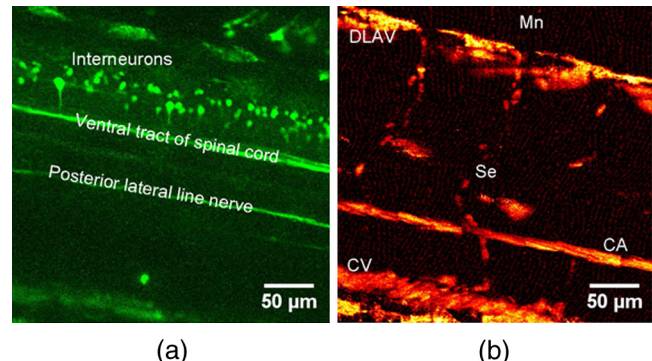
The imaging results of the moss leaves are shown in Fig. 4. By two-photon microscopy, both leaf cell boundaries and chloroplasts inside of leaf cells are shown in Fig. 4(a). Bright red fluorescence signal from chloroplasts and some red autofluorescence signals are shown in confocal image [Fig. 4(b)]. Figures 4(c) and 4(d) show the OR-PAM MAP image of the leaves at 570 and 578 nm wavelengths separately. In addition to chloroplasts, the OR-PAM MAP images also reveal details of unknown, nonfluorescent chromophores in the leaves. In the trimodality moss leaf image [Fig. 4(e)], the confocal image, the two-photon image, and the 570-nm OR-PAM MAP image are merged into red, green, and blue color channels separately. Some unknown, nonfluorescent chromophores that are not revealed by fluorescence images in red and green
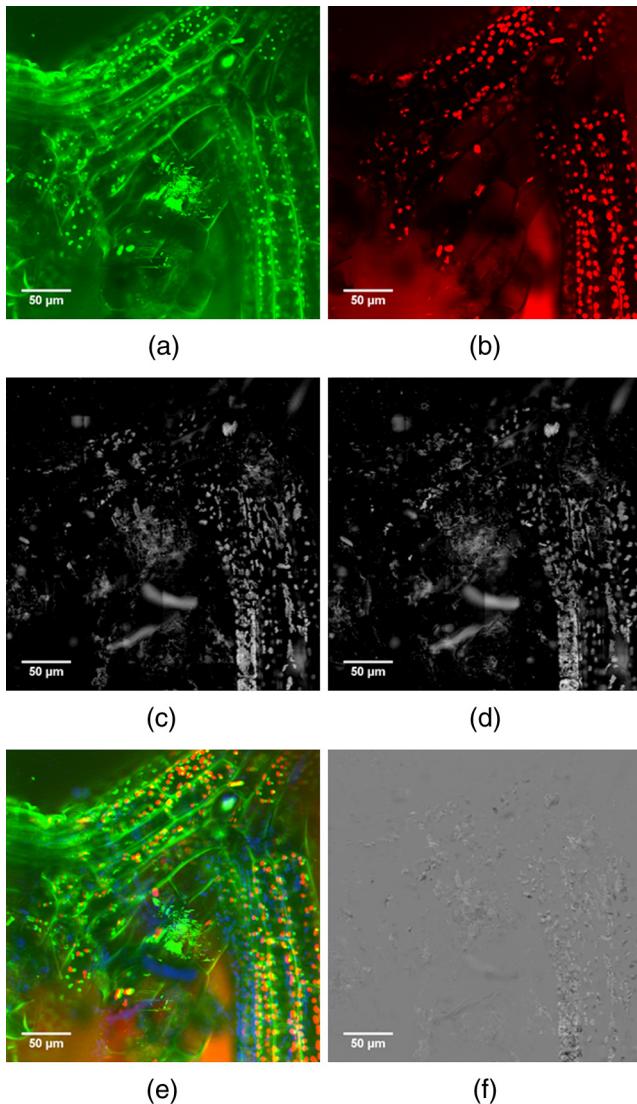
Fig. 4 Two-photon (a), confocal (b), and optical-resolution photoacoustic [(c) and (d)] microscopy images acquired with wild-type moss leaves. Excitation wavelengths of 570 and 578 nm were used to generate (c) and (d) separately. A merged trimodality image (e) was rendered from (a) to (c). Although chloroplasts can be seen by three modalities, complementary features of chloroplasts are surprisingly shown in (e). The unknown, nonfluorescent chromophores that were not revealed by fluorescence images in the red and green channels can be seen in blue channel of (e). A differential absorption contrast (DAC) OR-PAM maximum amplitude projection image (f) was generated from (c) to (d). With the selection of appropriate wavelengths, DAC OR-PAM images may reveal *in vivo* functional information of nonfluorescent chromophores.

channels can be identified by blue channel in the merged image [Fig. 4(e)]. To show the optical absorption difference at different wavelengths, we first subtracted Fig. 4(d) from Fig. 4(c) pixel by pixel. In the second step, we generated the differential absorption contrast (DAC) of the OR-PAM MAP image [Fig. 4(f)] by remapping the subtracted pixel gray-scale values to 0 to 255. DAC-OR-PAM imaging can be powerful because when appropriate wavelengths are selected, it can reveal *in vivo* functional information of nonfluorescent chromophores. For example, oxygenated hemoglobin can be easily differentiated from deoxygenated hemoglobin by choosing two different laser wavelengths.

Confocal and two-photon fluorescence microscopies have been widely used for almost half a century. The abundant, commercially available fluorescence dyes customized for labeling different chromophores are the major strength of confocal and two-photon fluorescence microscopies, in addition to their distinct technical features. OR-PAM is a new optical microscopy technology. Its major technology specifications, such as imaging speed, signal-to-noise ratio, and resolution, have been significantly improved since its invention in 2008 and will continue to improve. Although OR-PAM's current major strength lies in its label-free optical absorption contrast, we envision that customized, nonfluorescent PA dyes will extend the applications of OR-PAM technology in the near future. As we demonstrated in the above three experiments, OR-PAM is a complementary technology that enriches the contrasts of confocal and two-photon fluorescence microscopy.

4 Conclusion

Fluorescence microscopies have become indispensable imaging modalities in biology and medicine, especially since the invention of GFP and other molecular probes. Although endogenous fluorophores, such as NADH/FAD, melanin, keratin, and elastin fibers, exist in biological samples, fluorescence microscopies in many applications still rely on the usage of exogenous fluorescent probes that may affect cellular structure and function. Label-free microscopy represents another trend in modern microscopy. OR-PAM can provide complementary, label-free optical absorption contrast and differential absorption contrast by imaging nonfluorescent chromophores in biological samples. Here, for the first time, we demonstrated how both fluorescent proteins and nonfluorescent chromophores can be imaged by a confocal, two-photon, and OR-PA microscopy platform. The innovative microscope provides a novel platform in a familiar microscopic fluorescence imaging setting for future biological and medical discoveries.

References

1. M. Chalfie et al., "Green fluorescent protein as a marker for gene expression," *Science* **263**(5148), 802–805 (1994).
2. R. Y. Tsien, "The green fluorescent protein," *Annu. Rev. Biochem.* **67**(1), 509–544 (1998).
3. S. Hu et al., "Functional transcranial brain imaging by optical-resolution photoacoustic microscopy," *J. Biomed. Opt.* **14**(4), 040503 (2009).
4. X. Zhang et al., "Simultaneous in vivo imaging of melanin and lipofuscin in the retina with photoacoustic ophthalmoscopy and autofluorescence imaging," *J. Biomed. Opt.* **16**(8), 080504 (2011).
5. C. Zhang et al., "Label-free photoacoustic microscopy of cytochromes," *J. Biomed. Opt.* **18**(2), 020504 (2013).

6. T. J. Allen et al., "Spectroscopic photoacoustic imaging of lipid-rich plaques in the human aorta in the 740 to 1400 nm wavelength range," *J. Biomed. Opt.* **17**(6), 061209 (2012).
7. Y. Wang et al., "Integrated photoacoustic and fluorescence confocal microscopy," *IEEE Trans. Biomed. Eng.* **57**(10), 2576–2578 (2010).
8. Y. Wang et al., "In vivo integrated photoacoustic and confocal microscopy of hemoglobin oxygen saturation and oxygen partial pressure," *Opt. Lett.* **36**(7), 1029–1031 (2011).
9. Z. Tan et al., "Multimodal subcellular imaging with microcavity photoacoustic transducer," *Opt. Express* **19**(3), 2426–2431 (2011).
10. P. Shao et al., "Integrated micro-endoscopy system for simultaneous fluorescence and optical-resolution photoacoustic imaging," *J. Biomed. Opt.* **17**(7), 076024 (2012).
11. S.-L. Chen et al., "A fiber-optic system for dual-modality photoacoustic microscopy and confocal fluorescence microscopy using miniature components," *Photoacoustics* **1**(2), 30–35 (2013).
12. F. Soto et al., "NGL-2 regulates pathway-specific neurite growth and lamination, synapse formation and signal transmission in the retina," *J. Neurosci.* **33**(29), 11949–11959 (2013).
13. L. M. Swanhart et al., "Characterization of an lhx1a transgenic reporter in zebrafish," *Int. J. Dev. Biol.* **54**(4), 731–736 (2010).
14. M. Westerfield, *The Zebrafish Book: A Guide for the Laboratory Use of Zebrafish (Danio Rerio)*, 4th ed., University of Oregon Press, Eugene (2000).

Bin Rao received his PhD in biomedical optics from Beckman Laser Institute & Medical Clinic (BLI-MC), University of California, Irvine, in 2008. The ophthalmic Doppler optical coherence tomography system out of his PhD work is being used in a clinical study at BLI-MC. His postdoctoral trainings at Washington University in Saint Louis include photoacoustic microscopy, confocal, and two-photon microscopy. He was awarded the NIH Pathway to Independence Award in 2012.

Florentina Soto received her PhD from University of Alicante in Spain in 1992. She was an independent group leader at the Max Planck Institute in Goettingen, Germany, and a visiting scientist at the University of Washington in Seattle before she joined Washington University in St. Louis in 2009 as a research assistant professor. Her main research interest is to understand the molecular basis of the development and maintenance of neuronal circuits in the retina.

Daniel Kerschensteiner received his MD degree from Georg August University in Göttingen, Germany, in 2004. He was a postdoctoral fellow at University College London, UK, and at University of Washington in Seattle before he was appointed as an assistant professor of ophthalmology and visual sciences and anatomy and neurobiology in 2009. His laboratory studies the development and function of neural circuits in the retina using a combination of imaging, electrophysiology and genetic approaches.

Lihong V. Wang holds the Beare Distinguished Professorship at Washington University. His book titled "Biomedical Optics" won the Goodman Award. He has published 365 journal articles with an h-index of 85 (>28,000 citations) and delivered 380 keynote/plenary/invited talks. His laboratory invented functional photoacoustic CT and 3-D photoacoustic microscopy. He serves as the editor-in-chief of the *Journal of Biomedical Optics*. He was awarded OSA's C.E.K. Mees Medal, NIH Director's Pioneer Award, and IEEE's Biomedical Engineering Award.